Jurnal Kejuruteraan 37(2) 2025: 771-780
https://doi.org/10.17576/jkukm-2025-37(2)-17

Effect of Point Distance and Time Exposure on Mechanical Properties of Selective Laser Melted Stainless Steel 316

Asa Fansuri Abu Samah[a], Rafidah Hasan[a,b*] & Zurina Shamsudin[a]

[a]*Fakulti Teknologi dan Kejuruteraan Mekanikal,*

Universiti Teknikal Malaysia Melaka, Hang Tuah Jaya, 76100 Durian Tunggal, Melaka, Malaysia

[b]*Centre for Advanced Research on Energy,*

Universiti Teknikal Malaysia Melaka, Hang Tuah Jaya, 76100 Durian Tunggal, Melaka, Malaysia

[*]*Corresponding author: rafidahhasan@utem.edu.my*

Received 9 January 2024, Received in revised form 4 October 2024
Accepted 4 November 2024, Available online 30 March 2025

ABSTRACT

This study investigates the effect of point distance and time exposure on SLM stainless steel 316 and compare with standard conventional stainless steel 316. Nine specimens (VD2, VD3/VT1, and VT2) were fabricated using the SLM machine Renishaw RenAM 500E with parameters of 240 W laser power, 0.055 mm and 0.06 mm point distance, 80 µs and 90 µs time exposure, 0.11 mm hatch distance, 0.05 mm layer thickness, 67° scanning rotation between subsequent layers, and a stripe with a 5 mm width scanning strategy. The shape of the particle is almost spherical, and the range of particle diameters of metallic powder was 15-45 µm for the fabrication of SLM stainless steel 316. Three specimens of stainless steel 316 from a conventional plate were prepared using a laser cutting machine. Twelve specimens were tested with the Archimedes method using an MDS-300 densimeter for density measurement, surface roughness test using a non-contact profilometer for surface roughness measurement, ultrasonic test using Olympus Epoch 650 to determine sound velocity measurement, and three-point bending test using Instron 5585 to determine Young's modulus value. In ultrasonic testing, results show that Young's modulus value of VD3/VT1 (129.152 GPa) is more comparable to the standard Young's modulus of stainless steel (193 GPa). This is due to a stable molten pool and coarse grain size which leads to an increase in density and sound velocity increase in SLM parts. In three-point bending testing, it is shown that Young's modulus value of VD3/VT1 (126.825 GPa) is comparable with standard Young's modulus value of stainless steel 316, due to the internal structure formed during the SLM process. From this study, it is shown that more analysis should be done to explore how point distance and time exposure can be factors that effect on mechanical properties.

Keywords: Selective laser melted; point distance; time exposure; mechanical properties; stainless steel 316

INTRODUCTION

Selective Laser Melted, also known as SLM, is an additive manufacturing method to form metallic parts in which a high powered laser beam is used. It can be used for repairing and restoring automotive components (Adil Habeeb et al. 2023). During the printing process, the laser beam melts and fuses metallic powders together. As the laser beam hits a thin layer of material, it selectively joins particles together. After one complete print cycle, the metallic parts are lowered by the precise amount of the thickness of a single layer and the SLM machine adds a new layer of powdered material to the previous one. Unused powder is manually removed from metallic part, and consequently the metallic part is removed from the substrate at the end of the printing process.

Stainless steel 316 is widely used as powder feedstock within SLM, due to its low cost compared to other powder, such as titanium powder (Alsalla et al. 2018). There are many studies in the literature on the effects of process parameters and build orientation of SLM stainless steel 316. Lackey et al. (2016) investigated the effect of build orientation of SLM stainless steel 316 on mechanical properties. It was found that SLM stainless steel 316 with a 0° orientation has similar mechanical properties to

standard conventional stainless steel 316 including tensile strength and Young's modulus, due to the arrangement of the build orientation arrangement compared to the 90° build orientation. Yusuf et al. (2017) conducted a study on SLM SS316 by using the powders with particle diameters ranging from 15 to 40 µm to study porosity and microhardness and found that high density (≥99 %) was achieved compared with standard density value of stainless steel 316, and average microhardness values in SLM specimens were higher than standard conventional stainless steel 316. This is due to fine microstructures from the fast solidification rate during the SLM process. Larimian et al. (2022) suggested that densification behavior of SLM stainless steel 316 parts depends on the scanning speed, layer thickness, and laser power. They observed that high laser energy density is obtained from low scan speed with high laser power, with low value of hatch distance and layer thickness, improves the densification behavior of fabricated parts. Cheng et al. (2016) studied the effect of scanning direction after each layer by applying different rotations (45°, 67° and 90°). They reported that rotation can reduce residual stress and result in warping of the SLM parts. Fu et al. (2021) studied comparison of mechanical properties in SLM 316 by micro and standard size laser beams. It was reported that micro laser beam specimens have a lower level of residual stress, due to a smaller molten pool and more thermal cycles.

This study investigates the effects of laser time exposure and point distance on mechanical properties of selective laser melted stainless steel 316 using ultrasonic testing and three-point bending.

METHODOLOGY

POWDER FEEDSTOCK

For VD2, VD3/VT1, and VT2 specimens, SS 316 L-0407 powder was used as feedstock for fabrication. Stainless steel 316 powder was supplied by 3DGens Sdn Bhd . The shape and range of particle size of the metallic powder are almost spherical and range from 15-45 µm, respectively. The chemical composition of SS 316 L-0407 powder is given in Table 1.

PREPARATION OF SPECIMENS

For SLM stainless steel 316, nine specimens of VD2, VD3/VT1, and VT2 were fabricated using the SLM machine Renishaw RenAM 500E. Nine specimens of SLM stainless steel 316 were made with process parameters as shown in Table 2. Every specimen ID had three specimens of SLM stainless steel 316. Scanning speed was calculated from Equation (1) and energy density was determined from Equation (2), where P is laser power (W), v is scan speed (mm/s), h is hatch distance (mm) and t is layer thickness (mm).

$$v = \frac{Point\ distance}{Time\ exposure} \tag{1}$$

$$ED = \frac{P}{vht} \tag{2}$$

The scanning strategy and scanning rotation between subsequent layers for the fabrication SLM stainless steel 316 are a stripe with 5 mm width and 67°, respectively. The dimension specimens of the SLM stainless steel 316 were rectangular with 100 mm length, 20 mm width, and 5 mm thickness according to ASTM E290 (2022) (Standard Test Methods for Bend Testing of Material for Ductility) as shown in Figure 1.

For standard conventional stainless steel 316, three specimens were prepared from a conventional plate using Amada FO-MII 3015NT Laser Cutting Machine. The dimension of the three specimens of conventional stainless steel 316 were also the same as the dimension of the SLM stainless steel 316 specimens.

In total, twelve specimens were fabricated, including nine specimens fabricated from SLM, and three specimens were prepared from the conventional plate.

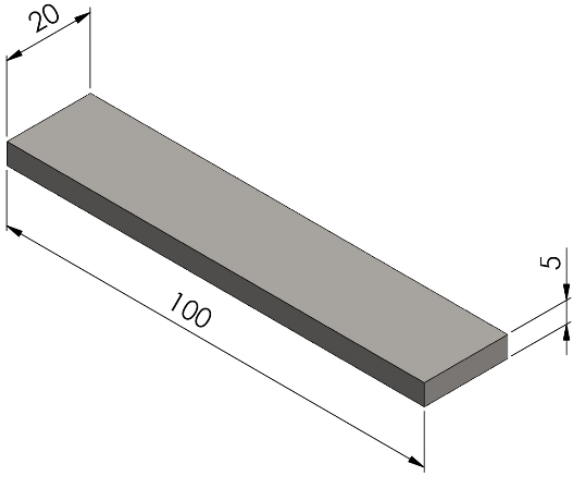

FIGURE 1. Schematic diagram of SLM stainless steel 316 specimens with dimensions

DENSITY MEASUREMENT

Standard conventional stainless steel 316 and SLM stainless steel 316 (VD2, VD3/VT1, and VT2) specimens were tested with an Electronic Densimeter MDS-300 for measuring density. All measurements were conducted with water at room temperature (approximately 25°C). For determining the density of each specimen, a total of three readings of density were obtained on every specimen, and the average density value was determined. For the theoretical value of density, the Archimedes method was used to calculate specimen density. The measured specimen's density is given in Equation (3), where ρ is the density of specimen, M_a is the measured mass of the specimens, measured in air, M_w is measured mass of the specimens measured in water, and ρ_w is the density of water.

$$\rho = \left(\frac{M_a}{M_a - M_w}\right)\rho_w \tag{3}$$

SURFACE ROUGHNESS

In this study, surface roughness was tested with a non-contact 3D Surface Profilometer from Shodensha GR3400. The magnification of this instrument was 10× with a Carl Zeiss microscope lens. Readings were obtained at three different positions (left position, center position, and right position) on the top surface of the specimens. WinRoof software was used for measuring surface roughness. A total of three readings of the surface roughness profile were determined for each specimen, and the average surface roughness value (Ra) was calculated.

ULTRASONIC TESTING

The velocity value of twelve specimens was determined from the ultrasonic test according to ASTM A578 (2023) (Standard Specification for Straight-Beam Ultrasonic Examination of Rolled Steel Plates for Special Applications). An olympus EPOCH 650 ultrasonic flaw detector was used to perform straight-beam ultrasonic testing by using the Pulse-Echo testing method. A single transducer (DL4R–3.5×10) was connected to the ultrasonic flaw detector for sending and receiving ultrasonic waves.

Calibration of the ultrasonic flaw detector was done by applying it on a calibration block prior to experiments. Calibration of the ultrasonic flaw detector must be done to verify the precision of the test results and ensure the proper functioning of the ultrasonic flaw detector. Data were recorded and calculated using Equation (5) which has been simplified from Eq. (4) to determine Young's Modulus where longitudinal waves V_L (m/s), material density ρ (kg/m^3), Young's Modulus E (GPa), and Poisson's ratio, ν (Hellier, 2012). Poisson's ratio for stainless steel 316 was taken from literature. The poisson ratio of stainless steel 316 is 0.28 (Olivas-Alanis et al. 2023).

$$V_L = \sqrt{\frac{E(1-\nu)}{\rho(1+\nu)(1-2\nu)}} \tag{4}$$

$$E = \frac{\rho V_L{}^2(1+\nu)(1-2\nu)}{(1-\nu)} \tag{5}$$

THREE-POINT BENDING TESTING

Young's modulus of twelve specimens was determined using an Instron 5585 testing machine. The span length between two lower supports for test specimens was 80 mm. Specimens were tested by bending to a 90° angle at room temperature and at 5 mm/min speed according to ASTM E290 (2022) (Standard Test Methods for Bend Testing of Material for Ductility). Bluehill software was used to record data from three-point bending of specimens.

Young's modulus of specimens was calculated for the three-point bending test using Equation (6), where Young's modulus E (GPa), distance between two lower supports L (mm), moment of inertia I (mm^4). Stiffness was calculated from slope of load-extension graph (Sato et al. 2006) as shown in Figure 2. For rectangular specimens, moment of inertia was calculated using Equation (7), where b is width and h is height of specimens.

$$E = \frac{L^3 \cdot stiffness}{48I} \tag{6}$$

$$I = \frac{bh^3}{12} \tag{7}$$

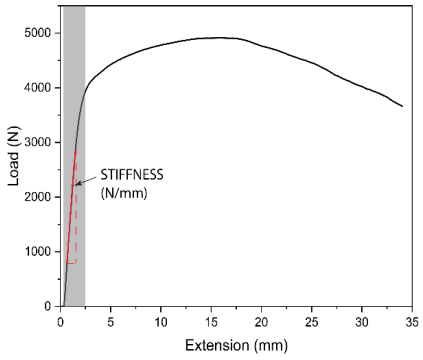

FIGURE 2. Load - extension graph of three point-bending test

TABLE 1. Chemical composition of SS 316 L-0407 powder

Element	Fe	Cr	Mo	Mn	Ni	Si	C	N	P	S
Wt %	Bal.	16.0 – 18.0	2.0 – 3.0	10.0 – 14.0	≤ 2.00	≤ 1.00	≤ 0.10	≤ 0.10	≤ 0.03	≤ 0.03

TABLE 2. Process parameters of SLM stainless steel 316

Parameter	VD2	VD3/VT1	VT2
Laser Power, P	240 W	240 W	240 W
Point Distance, d	0.055 mm	0.06 mm	0.06 mm
Exposure Time, T	80 µs	80 µs	90 µs
Scanning Speed, v	687.50 mm/s	750.00 mm/s	666.67 mm/s
Hatch Distance, h	0.11 mm	0.11 mm	0.11 mm
Layer Thickness, t	0.05 mm	0.05 mm	0.05 mm
Energy Density, ED	63.47 J/mm^3	58.18 J/mm^3	65.45 J/mm^3

RESULTS AND DISCUSSION

DENSITY OF SPECIMENS

Table 3 shows the density of SLM stainless steel 316, conventional stainless steel 316, and literature compared with the standard density of stainless steel 316 (Davis 1998). VT2 specimen is more comparable with standard density of stainless steel 316, which percentage difference of 1.26 %. On the other hand, VD3/VT1 specimen has lower density value compared with the standard value.

Remaining porosity in SLM stainless steel 316 was hard to avoid, due to powder spattering during the SLM process (Pal et al. 2020). High scanning speed increases the spattering of raw powder particles, which adds to the number of spattered particles at the beginning of the samples. Inert gas mixes with molten metal from the interparticle space. Then, bubble moves following the vortex of the melt pool. Bubbles may go out of the melt pool or remain inside the vortex. As the melt pool solidifies from bottom to the upper part of the melt pool, the vortex also becomes smaller and moves upward. Bubble also moves up with the vortex. Eventually, bubbles remain exposed as open pores, or may just stay below the top surface having a tiny layer, as shown in Figure 3.

VT2 specimen has a high density in SLM stainless steel 316, due to the states of the molten pool during the SLM process (Huang et al. 2020; Larimian et al. 2022). A lower scanning speed during the SLM process which increases the time exposure and the decreases point distance, allows the laser beam to stay longer on metal powder to receive heat energy, which leads to more stable melt pools and fully melted metallic powder. Therefore, density, strength, and Young's modulus of SLM metallic parts increase, due to the decreased porosity and internal void. However, when the scanning speed is too low, it leads excessive heat energy being absorbed by the metal powder and the molten pool in an unstable state will cause the powder to vaporize and form pores which causes the density of metallic parts to decrease.

SURFACE ROUGHNESS OF SPECIMENS

Table 4 shows the results of surface roughness for tested specimens and other literature. It shows that the surface roughness of the VD3/VT1 specimen has the lowest value among SLM stainless steel 316, which percentage difference is 51.23 % compared with the standard conventional SS 316. Meanwhile, the VD2 specimen has higher average surface roughness compared to VD3/VT1, VT2, and the standard conventional SS 316, with percentage difference of 18.90 %, 12.32 %, and 68.47 %, respectively. However, the VD2 specimen has lower average surface roughness than Jagdale et al. (2022) and Woźniak et al. (2020), with percentage difference is 41.82 % and 30.16 %, respectively.

High surface roughness of SLM stainless steel 316 is due to insufficient energy input for fully melting the powder under high point distance and lower time exposure, which results in high scanning speed, and the balling phenomenon occuring during SLM print processing, leading to unstable and wrinkled surface of SLM parts (Guo et al. 2019; Sun et al. 2020). During the process, high point distance and low time exposure result in the laser beam being fired for a short duration on metal powder. Metal powder is not fully melted and decreases its wettability to spread on the substrate as shown in Figure 4. High point distance and high time exposure, which are associated with low scanning speed can provide sufficient energy input, thus resulting in a high temperature of the molten pool and long liquid lifetime. High temperature in the molten pool enhances wettability and spreading on the substrate. It can contribute to a decrease in surface roughness of SLM parts.

SOUND VELOCITY OF SPECIMENS

The result of the average sound velocity from the ultrasonic test is shown in Table 5. The standard sound velocity of stainless steel 316 was obtained from the manufacturer datasheet (Pan American Industries Inc., n.d.) It shows that the VD3/VT1 specimen is more comparable with the standard sound velocity of stainless steel 316, and Khan et al. (2016), of which the percentage difference of sound velocity is 8.15 %, and 10.12 %, respectively. The VT2 specimen has the lowest sound velocity value, with a 9.38 % percentage difference compared to standard sound velocity of stainless steel 316 and 11.36 % percentage difference compared to Khan et al. (2016). This is due to the grain size of stainless steel 316. As reported in the literature (Bouda et al. 2003), it has been stated that an increase in grain border area, which means a decrease in grain size, leads to an increase in the scattering of ultrasonic waves. High point distance and low time exposure in the SLM process parameters, where the laser beam stays on the metal powder for a shorter period of time, mean that the grain size of the materials decreases because of faster cooling rates during the SLM process (Hao et al. 2023), as shown in Figure 5. This means that ultrasonic waves need to travel longer distances along the small grain sizes to cover the material thickness, which makes the sound velocity decrease.

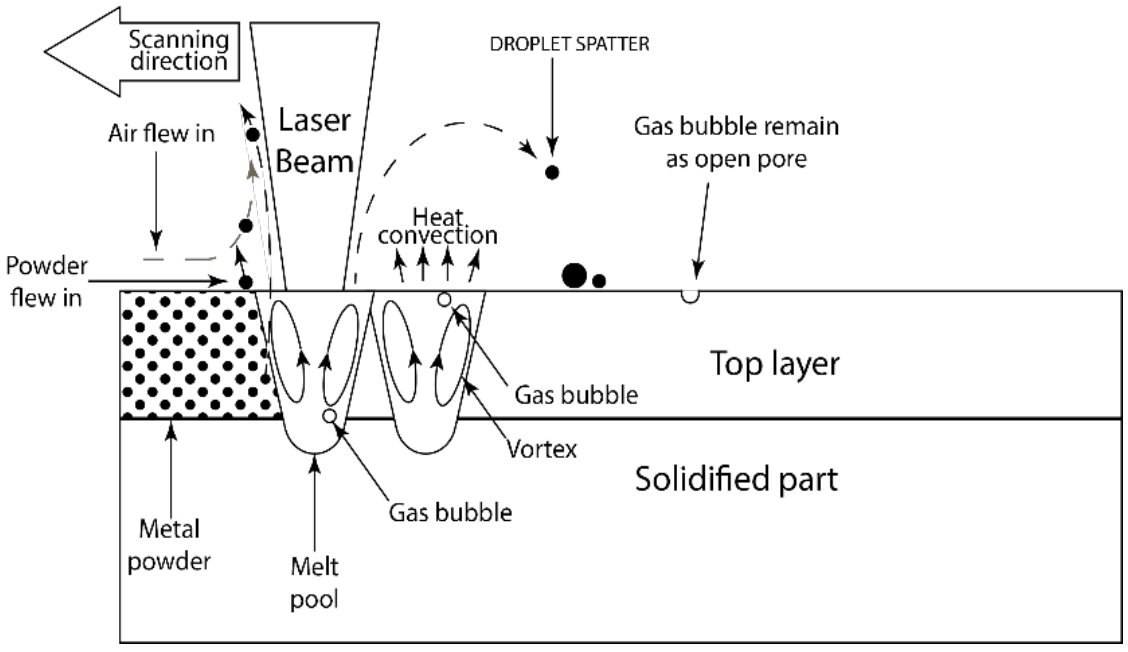

FIGURE 3. Schematic diagram of pore formation in SLM process (adapted from Pal et al. 2020)

TABLE 3. Result of average density for tested specimens

SPECIMEN ID	Measured average density,	Standard density of stainless steel 316 (Davis, 1998)	Percentage difference
VD2	7.898 g/cm^3	8.0 g/cm^3	1.28 %
VD3/VT1	7.896 g/cm^3		1.3 %
VT2	7.899 g/cm^3		1.26 %
Standard conventional SS 316	7.919 g/cm^3		1.01 %
Peng et al. (2018)	7.910 g/cm^3		1.12 %
Cherry et al. (2015)	7.704 g/cm^3		3.70 %

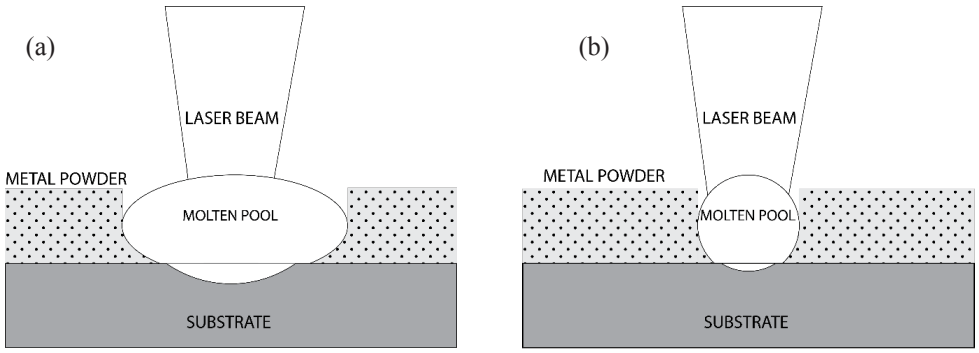

FIGURE 4. Schematic diagram of balling effect (a) large wetting area and (b) small wetting area during SLM processing (adapted from Li et al. 2012)

TABLE 4. Result of average surface roughness for tested specimens

SPECIMEN ID	Average Surface roughness, Ra (μm)
VD2	2.878 ± 0.827 μm
VD3/VT1	2.381 ± 0.543 μm
VT2	2.544 ± 0.549 μm
Standard conventional SS 316	1.410 ± 0.181 μm
Woźniak et al. (2020)	3.90 ± 0.10 μm
Jagdale et al. (2022)	4.40 ± 1.67 μm

YOUNG'S MODULUS OF SPECIMENS

The result of the average Young's Modulus from the ultrasonic test and three-point bending test as shown in Table 6. Standard Young's modulus of stainless steel 316 was obtained from Matweb (Davis, 1998). In ultrasonic testing, it shows that the VD3/VT1 specimen is more comparable to the standard Young's modulus of stainless steel 316 and Victoria et al. (2015), with a percentage difference of 10.97 % and 18.89 %, respectively. The value from the three-point bending test derived from Equation 5 shows that the VD3/VT1 specimen is higher than other specimens and literature, with a percentage difference of 42.26 % compared to the Young's modulus standard value of stainless steel 316. In the results from Bluehill software for the three-point bending test, the Young's modulus value of the VD3/VT1 specimen was also comparable to the standard Young's modulus of stainless steel 316, with a percentage difference of 41.38 %. Also, the Young's modulus value of VD3/VT1 is higher than that reported by Kozub et al. (2022), with a percentage difference of stainless steel 316 from Kozub et al. compared to standard Young's modulus stainless steel 316 is 16.03 %, due to low internal defects of SLM metal parts.

In the literature (Chen et al. 2022; Guan et al. 2013) it is suggested that the mechanical properties of SLM part's mechanical properties are related to internal defects such as unmetled powder particles, pores, and cracks due to faster laser shift speed, which cannot completely melt metal powder. High scanning speed in process parameters with ideal laser power can increase the mechanical properties of SLM parts, with a high value of point distance with lower laser time exposure in scanning speed to melt metal powder. However, excessive scanning speed could lead to an increase in cooling rate causing poor quality and a decrease in mechanical properties. Also, Chen et al. (2019) suggested that higher scanning speed leads to defects in the internal structure of metal parts. When the scan speed is higher, the width of overlap between two solidified areas decrease, which leads to holes forming and cracking in SLM parts due to insufficient laser energy and decreased mechanical properties.

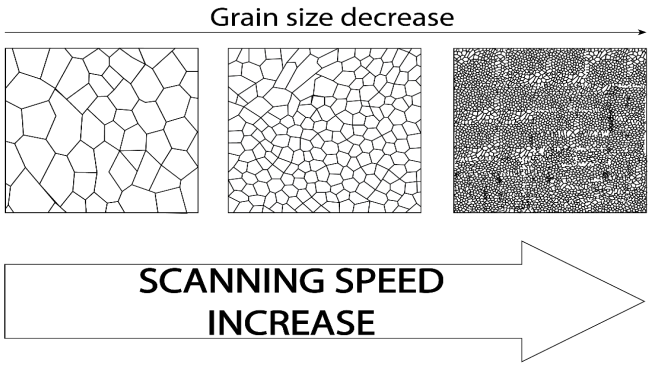

FIGURE 5. Effect of scanning speed on grain size of SLM stainless steel 316 (adapted from Hao et al. 2023)

TABLE 5. Result of average sound velocity for tested specimens

SPECIMEN ID	Sound velocity (m/s)	Standard sound velocity of stainless steel 316 (Pan American Industries Inc.)
VD2	5265.444 m/s	
VD3/VT1	5290.667 m/s	
VT2	5225.667 m/s	5740.40 m/s
Standard conventional SS 316	5557.110 m/s	
Khan et al. (2016)	5855.000 m/s	

TABLE 6. Result of average Young's Modulus for tested specimens

SPECIMEN ID	Average Young's Modulus (GPa)			Standard Young's Modulus of Stainless Steel 316 (Davis, 1998)
	Ultrasonic Testing	Three-point bending testing		
		Value from Equation 5	Value from Bluehill software	
VD2	171.340 GPa	113.219 GPa	117.607 GPa	193 GPa
VD3/VT1	172.930 GPa	125.667 GPa	126.825 GPa	
VT2	168.795 GPa	119.358 GPa	122.802 GPa	
Standard conventional SS 316	191.327 GPa	86.943 GPa	93.347 GPa	
Kozub et al. (2022)	-	108 GPa		
Victoria et al. (2015)	209 GPa	-		

RELATIONSHIP BETWEEN YOUNG'S MODULUS AND AVERAGE SURFACE ROUGHNESS

Figure 6 (a) shows the relationship between Young's Modulus and average surface roughness. It shows that Young's modulus from the ultrasonic test slightly decreases with an increase average surface roughness. For the three-point bending test, Young's modulus decreased with an increase in average surface roughness in specimens of SLM stainless steel 316 because of high stress concentration. High stress concentration occurs by dislocation pileup from coarse grain formation in the material.

Renzo et al. (2022) reported that a rough surface on SLM parts can be considered a natural micro-notch, where local stress concentration promotes crack initiation and propagation. SLM produces as-built parts with a rough surface depending on process parameters. High scanning speed produces high surface roughness of SLM parts due to the molten layer solidification rate. Defects occur in partially molten particles with powder and created a solidified shape of the laser scanning track. Micro-cracks and the balling effect increase surface roughness of SLM parts.

RELATIONSHIP BETWEEN YOUNG'S MODULUS AND AVERAGE ENERGY DENSITY

Figure 6 (b) shows the relationship between Young's modulus and energy density with constant laser power, hatch distance and layer thickness, which is represented by a dashed line for the linear line of Young's modulus. For the ultrasonic test, it shows that the value of Young's modulus decreases slightly with an increase of energy density in the process parameters. For the three-point bending test, Young's modulus value decreased as energy density increased from 58.18 J/mm^3 to 63.47 J/mm^3, and Young's modulus increased after energy density increased from 63.47 J/mm^3 to 65.45 J/mm^3.

Montero-Sistiaga et al. (2018) reported that when all other parameters are constant, increasing scanning speed results in an insufficient size of melt pools, leading to increasing porosity and decreasing density of SLM parts. Increasing scanning speed, which increases point distance and decrease time exposure reduces energy density and results in insufficient re-melting of the previous layer and poor bonding between the upper layer and the bottom layer which causes the mechanical properties of SLM parts to decrease. Also, high cooling rates that follow the heating of specimens in a short period of time leads to high thermal gradient that causes micro and macro cracks that lower the final density of the built part.

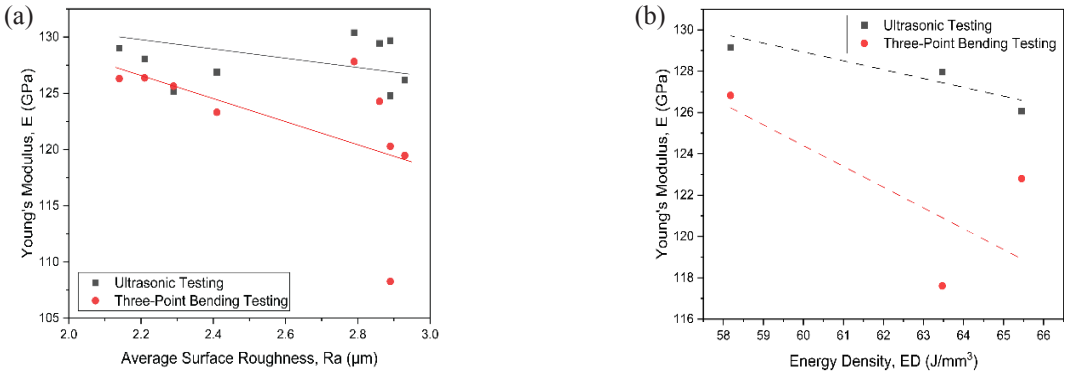

FIGURE 6. Scatter plots graph of (a) relationship between Young's Modulus and average surface roughness and line graph of (b) relationship between Young's Modulus and energy density

CONCLUSION

The overall results discussed in this paper show that the VD3/VT1 specimen is more comparable to standard stainless steel 316 than the VD2 and VT2 specimens in density, sound velocity of ultrasonic waves and Young's modulus using the ultrasonic test and three-point bending test. VD3/VT1 specimen had a high point distance and low time exposure, which were 0.06 mm point distance and 80 μs time exposure with constant laser power, hatch distance, and layer thickness in the process parameters for stable melting of powder to increase mechanical properties of SLM stainless steel 316.

With a lower point distance and higher time exposure, the lower scanning speeds and longer laser stays on metal

powder leads to excessive heat energy during process, which leads to a decrease in mechanical properties of SLM stainless steel 316. When the point distance is lower than 0.06 mm, the Young's modulus of SLM parts decreases. When the time exposure value is greater than 80 µs, the Young's modulus of SLM parts also decreases. It can be concluded that VD3/VT1 specimen has a stable melt pool to melt metal powder during the process.

From this study, it is shown that more analysis should be done where point distance and time exposure can be factors that affect mechanical properties in the nearest future.

ACKNOWLEDGEMENT

This study is funded by Ministry of Higher Education (MOHE) of Malaysia through the Fundamental Research Grant Scheme (FRGS), No: FRGS/1/2022/TK10/UTeM/02/20. The authors also would like to thank Universiti Teknikal Malaysia Melaka (UTeM) for all the supports. This work has initially been accepted and presented at the International Conferences 7th Powder Metallurgy (PM7) and Advanced Processes & Systems in Manufacturing (APSIM 2023). Also, this paper is the full paper of an extended abstract of International Conferences 7th Powder Metallurgy (PM7) and Advanced Processes & Systems in Manufacturing (APSIM 2023).

DECLARATION OF COMPETING INTEREST

None.

REFERENCES

Alsalla, H. H., Smith, C., & Hao, L. 2018. Effect of build orientation on the surface quality, microstructure and mechanical properties of selective laser melting 316L stainless steel. *Rapid Prototyping Journal* 24(1): 9–17. https://doi.org/10.1108/RPJ-04-2016-0068

ASTM E290: test methods for bend testing of material for ductility. 2022. ASTM International. https://doi.org/10.1520/e0290-14

ASTM A578: specification for straight-beam ultrasonic examination of rolled steel plates for special applications. 2023. ASTM International. https://doi.org/10.1520/a0578_a0578m-17

Badidi Bouda, A., Lebaili, S., & Benchaala, A. 2003. Grain size influence on ultrasonic velocities and attenuation. *NDT & E International* 36(1): 1–5. https://doi.org/https://doi.org/10.1016/S0963-8695(02)00043-9

Chen, J., Wang, X., & Pan, Y. 2019. Influence of laser power and scan speed on the microstructure and properties of GH4169 alloy prepared by selective laser melting. *IOP Conference Series: Materials Science and Engineering* 688(3): 033064. https://doi.org/10.1088/1757-899X/688/3/033064

Chen, Z., Lu, Y., Luo, F., Zhang, S., Wei, P., Yao, S., & Wang, Y. 2022. Effect of laser scanning speed on the microstructure and mechanical properties of laser-powder-bed-fused k418 nickel-based alloy. *Materials (Basel)* 15(9): 3045.

Cheng, B., Shrestha, S., & Chou, K. 2016. Stress and deformation evaluations of scanning strategy effect in selective laser melting. *Additive Manufacturing* 12(8), 240–251. https://doi.org/10.1016/j.addma.2016.05.007

Cherry, J. A., Davies, H. M., Mehmood, S., Lavery, N. P., Brown, S. G. R., & Sienz, J. 2015. Investigation into the effect of process parameters on microstructural and physical properties of 316L stainless steel parts by selective laser melting. *The International Journal of Advanced Manufacturing Technology* 76(5), 869–879. https://doi.org/10.1007/s00170-014-6297-2

Davis, J. R. 1998. Engineering data for metals and alloys. ASM International. *Metals Handbook Desk Edition*. 64–84.

Fu, J., Qu, S., Ding, J., Song, X., & Fu, M. W. 2021. Comparison of the microstructure, mechanical properties and distortion of stainless steel 316 L fabricated by micro and conventional laser powder bed fusion. *Additive Manufacturing* 44: 102067. https://doi.org/https://doi.org/10.1016/j.addma.2021.102067

Guan, K., Wang, Z., Gao, M., Li, X., & Zeng, X. 2013. Effects of processing parameters on tensile properties of selective laser melted 304 stainless steel. *Materials & Design* 50: 581–586. https://doi.org/https://doi.org/10.1016/j.matdes.2013.03.056

Guo, M., Gu, D., Xi, L., Du, L., Zhang, H., & Zhang, J. 2019. Formation of scanning tracks during selective laser melting (SLM) of pure tungsten powder: morphology, geometric features and forming mechanisms. *International Journal of Refractory Metals and Hard Materials* 79: 37–46. https://doi.org/https://doi.org/10.1016/j.ijrmhm.2018.11.003

Hao, L., Wang, W., Zeng, J., Song, M., Chang, S., & Zhu, C. 2023. Effect of scanning speed and laser power on formability, microstructure, and quality of 316L stainless steel prepared by selective laser melting. *Journal of Materials Research and Technology* 25: 3189–3199. https://doi.org/https://doi.org/10.1016/j.jmrt.2023.06.144

Hellier, C. 2012. *Handbook of Nondestructive Evaluation*. 7.10-7.11.

Huang, W., Zhang, W., & Chen, X. 2020. Effect of SLM process parameters on relative density of maraging steel (18Ni-300) formed parts. *IOP Conference Series: Materials Science and Engineering* 774(1): 12027. https://doi.org/10.1088/1757-899X/774/1/012027

Jagdale, S. H., Theeda, S., Ravichander, B. B., & Kumar, G. 2022. Surface morphology and hardness of powder bed fused SS316L as a function of process parameters. *Solid Freeform Fabrication 2022: Proceedings of the 33rd Annual International Solid Freeform Fabrication Symposium – An Additive Manufacturing Conference*: 416-426.

Khan, S.Z., Khan, T.M., Joya, Y.F., Khan, M.A., Ahmed, S., & Shah, A. 2016. Assessment of material properties of AISI 316L stainless steel using non-destructive testing. *Nondestructive Testing and Evaluation* 31: 360-370.
https://doi.org/10.1080/10589759.2015.1121265

Kozub, B., Uthayakumar, M., & Kazior, J. 2022. The influence of nanographite addition on the compaction process and properties of AISI 316L sintered stainless steel. *Materials 15*(10): 3629. https://doi.org/10.3390/ma15103629

Lackey, A. D., & Stone, W. 2016. Comparative study of mechanical properties of 316L stainless steel between traditional production methods and selective laser melting. In *ProQuest Dissertations and Theses*. https://libproxy.utem.edu.my/login?url=https://www.proquest.com/dissertations-theses/comparative-study-mechanical-properties-316l/docview/1789297918/se-2?accountid=34984

Larimian, T., AlMangour, B., Grzesiak, D., Walunj, G., & Borkar, T. 2022. Effect of laser spot size, scanning strategy, scanning speed, and laser power on microstructure and mechanical behavior of 316L stainless steel fabricated via selective laser melting. *Journal of Materials Engineering and Performance* 31(3): 2205–2224. https://doi.org/10.1007/s11665-021-06387-8

Li, R., Liu, J., Shi, Y. 2012. Balling behavior of stainless steel and nickel powder during selective laser melting process. *Int J Adv Manuf Technol* 59: 1025–1035. https://doi.org/10.1007/s00170-011-3566-1

Montero-Sistiaga, M. L., Godino-Martinez, M., Boschmans, K., Kruth, J.-P., Van Humbeeck, J., & Vanmeensel, K. 2018. Microstructure evolution of 316L produced by HP-SLM (high power selective laser melting). *Additive Manufacturing* 23: 402–410. https://doi.org/10.1016/j.addma.2018.08.028

Olivas-Alanis, L. H., Abraham Fraga-Martínez, A., García-López, E., Lopez-Botello, O., Vazquez-Lepe, E., Cuan-Urquizo, E., & Rodriguez, C. A. 2023. Mechanical properties of AISI 316L lattice structures via laser powder bed fusion as a function of unit cell features. *Materials* 16(3): 1025. https://doi.org/10.3390/ma16031025

Pal, S., Lojen, G., Hudak, R., Rajtukova, V., Brajlih, T., Kokol, V., & Drstvenšek, I. 2020. As-fabricated surface morphologies of Ti-6Al-4V samples fabricated by different laser processing parameters in selective laser melting. *Additive Manufacturing* 33: 101147. https://doi.org/10.1016/j.addma.2020.101147

Pan American Industries Inc. n.d.. *Ultrasound Velocity of Material*. Retrieved November 30, 2023, from https://www.panamiris.com/downloads/UltrasoundVelocity.pdf

Peng, T., & Chen, C. 2018. Influence of energy density on energy demand and porosity of 316L stainless steel fabricated by selective laser melting. *International Journal of Precision Engineering and Manufacturing-Green Technology* 5(1): 55–62. https://doi.org/10.1007/s40684-018-0006-9

Renzo, D. A., Maletta, C., Sgambitterra, E., Furgiuele, F., & Berto, F. 2022. Surface roughness effect on multiaxial fatigue behavior of additively manufactured Ti6Al4V alloy. *International Journal of Fatigue* 163: 107022. https://doi.org/https://doi.org/10.1016/j.ijfatigue.2022.107022

Sato, T., Katagiri, K., Hokari, T., Hatakeyama, Y., Murakami, A., Nyilas, A., Kasaba, K., Teshima, H., & Hirano, H. 2006. Evaluation of Young's modulus of RE123 bulk superconductors by three point bending tests. *Physica C: Superconductivity and Its Applications* 445–448(1–2): 422–426. https://doi.org/10.1016/j.physc.2006.04.029

Sun, K., Peng, W., Yang, L., & Fang, L. 2020. Effect of SLM processing parameters on microstructures and mechanical properties of Al0.5CoCrFeNi high entropy alloys. *Metals* 10(2): 292. https://doi.org/10.3390/met10020292

Victoria, B., George, G., & Babu, V. (2015). Ultrasonic characterization of austenitic stainless steel in thermal variations. *J. IJSRSET* 1(6): 123-126.
https://doi.org/10.32628/IJSRSET151615

Woźniak, A., Adamiak, M., Chladek, G., & Kasperski, J. 2020. The influence of the process parameters on the microstructure and properties SLM processed 316 L stainless steel. *Archives of Metallurgy and Materials* 65(1): 17–80. https://doi.org/10.24425/amm.2019.131098

Yusuf, S. M., Chen, Y., Boardman, R., Yang, S., & Gao, N. 2017. Investigation on porosity and microhardness of 316L stainless steel fabricated by selective laser melting. *Metals 7*(2): 64. https://doi.org/10.3390/met7020064